COMPARING THE SOLUBILITY PRODUCTS OF LAYERED Me(II)-Al(III)-

HYDROXIDES BASED ON SORPTION STUDIES WITH Ni(II), Zn(II), Co(II), Fe(II),

AND Mn(II)

by

LASITA BHATTACHARYA

A Dissertation submitted to the

Graduate School-Newark

Rutgers, The State University of New Jersey

in partial fulfillment of the requirements

for the degree of

Master of Science

Graduate Program in Environmental Sciences

written under the direction of

Dr. Evert J. Elzinga

and approved by

_____

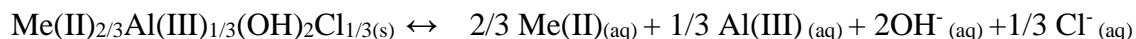_____

_____

Newark, New Jersey

October, 2017

©[2017]

Lasita Bhattacharya

Comparing the solubility products of layered Me(II)-Al(III)-hydroxides based on sorption

studies with Ni(II), Zn(II), Co(II), Fe(II), and Mn(II)

By Lasita Bhattacharya

Thesis Director: Dr. Evert J. Elzinga

The sorption of divalent metals onto Al-oxide sorbents may lead to the formation of

mixed metal-aluminum layered double hydroxide (Me(II)-Al(III)-LDH) phases. The

formation of these secondary phases may represents a significant pathway of

sequestration of various divalent metals, including Ni(II), Zn(II), Co(II), Fe(II) and

Mn(II), in aqueous geochemical environments such as soils and sediments. Despite of

their importance in metal sequestration there is not enough thermodynamic data available

to model their behavior in geochemical environment. Thus this study was designed to

estimate the solubility product values of Me(II)-Al(III)-LDH precipitates formed by

Ni(II), Zn(II), Co(II), Fe(II) and Mn(II) during sorption onto Al-oxide at near neutral and

alkaline pH value in NaCl electrolyte. Detailed kinetic studies were conducted to monitor

the sorption of these divalent metals onto γ-Al$_2$O$_3$. Equilibrium aqueous metal

concentrations were used to calculate the solubility products (Ksp) of the Me(II)-Al(III)-

LDH phases for the aqueous chemical equilibrium described by:

$$\text{Me(II)}_{2/3}\text{Al(III)}_{1/3}(\text{OH})_2\text{Cl}_{1/3(s)} \leftrightarrow 2/3 \text{ Me(II)}_{(aq)} + 1/3 \text{ Al(III)}_{(aq)} + 2\text{OH}^-_{(aq)} + 1/3 \text{ Cl}^-_{(aq)}$$

The Ksp values of the five metals span three orders of magnitude, indicating substantial

differences in the favorability of Me(II)-Al(III)-LDH precipitation, which increases in

the order Mn(II)<Fe(II)<Co(II)<Zn(II)<Ni(II). A linear relation is observed between the

Ksp values of the Me(II)-Al(III)-LDH and those of the corresponding β-Me(OH)$_2$ phases,

indicating that the substitution of Al(III) in the brucitic β-Me(OH)$_2$ lattice influences the stability of the resulting Me(II)-Al(III)-LDH phase in a fashion that is independent of the size of Al(III) relative to Me(II). The thermodynamic data obtained from our study demonstrate that the chloride-interlayered Me(II)-Al(III)-LDH phases characterized here have a higher solubility than MeCO$_3$ phases in a model groundwater system and in a calcitic system. Additional thermodynamic studies are needed to determine the impacts of environmentally relevant anions, particularly carbonate and silicate, on the formation and stability of Me(II)-Al(III)-LDH phases.

AKNOWLEDGEMENTS

Table of Contents

LIST OF TABLES

INTRODUCTION

In aqueous geochemical systems such as soils and sediments, sorption reactions at mineral-water interfaces significantly affect the mobility, speciation and bioavailability of trace metals. Iron- and Al-oxides and phyllosilicates are particularly important sorbents capable of metal sequestration through various mechanisms, including surface adsorption and precipitation reactions[1-8]. Recent studies have shown that the adsorption of divalent metals (Me(III)) onto Al-bearing mineral substrates may lead to the formation of Me(II)-Al(III)-layered double hydroxide (LDH) phases. These secondary precipitates consist of brucite-like $[Me^{II}(OH)_2]$ layers with partial isomorphous substitution of Al(III) for Me(II), where Al(III) is derived from the weathering of the mineral sorbent. The substitution of Al(III) for Me(II) in the trioctahedral metal-hydroxide sheets generates a net positive layer charge, which is neutralized by interlayer anions such as nitrate, chloride, carbonate and sulfate.[2, 9]. The resulting layered minerals have the general formula $Me^{II}_{1-x}Al^{III}_x (OH)_2(A^{n-})_{x/n} \cdot nH_2O$, where Me is the metal cation (Co, Zn, Ni, Fe etc) and A are the interlayer anions; x represents the extent of aluminum substitution which varies from 0.2 to 0.35[2, 9]. Because these precipitates form on a time scale similar to adsorption reactions [2, 3, 5, 10-13] they potentially play an important role in the removal of metal ions from solution. These phases have been observed in laboratory based model systems using metal oxides and various clay minerals as adsorbents [3, 5, 6, 8, 10, 12-17] and recent research has also identified the presence of mixed Ni(II)-, and Zn(II)-Al(III)-hydroxide phases in contaminated whole soils[18-23], implying that these minerals represents an important control on the solubility and mobility of Ni(II) and Zn(II) in these systems.

Although it has been identified that in the presence of Al-bearing mineral substrates, these mixed metal(II)-Al(III)-hydroxide phases precipitate on time scales of minutes and is thermodynamically favorable over the precipitation of pure $Me(OH)_2$ under typical soil conditions[2, 9, 18, 19, 24], there is not many studies on the thermodynamics of these minerals. Previous works include Peltier et al.[18] where the solubility product values of different Ni(II)-Al(III)-LDH phases were calculated from their respective free energies of formation. Relative stability of Ni(II)-Al(III)-LDH phases based on their interlayer species were estimated as well as compared with the stability of pure Ni hydroxides. Regelink and Temminghoff[25] calculated the solubility product values of Ni(II)-Al(III)-LDH phase using the ion activities, where calculations were done both with and without the interlayer anion activities and produced different values. Johnson and Glasser[9] estimated the solubility product values of different Me(II)-Al(III)-LDH phases where Me(II)= Ni, Zn, Co and Mg and conducted model calculations to show that the LDH phases are thermodynamically more stable than their corresponding divalent hydroxides. Thus considering the lack of thermodynamic data currently available for Me(II)-Al(III)-LDH phases, we designed the current study to estimate and compare the solubility products of Me(II)-Al(III)-LDH precipitates formed by Ni(II), Zn(II), Co(II), Fe(II) and Mn(II) during sorption onto Al-oxide at near neutral and alkaline pH values. This estimation of Ksp values for Me(II)-Al(III)-LDH phases is of particular importance as currently there is no established thermodynamic database existed for these minerals. Hence, the results of this study can be used as an important resource and can be incorporated in future studies involving similar Me(II)-Al(III)-LDH phases.

Therefore the objectives of this study can be summarized as-1. Investigating the long term kinetics of the Me(II)-γAl_2O_3 (Me= Ni, Zn, Co, Fe, and Mn) sorption experiments as a function of pH and 2. Estimate the solubility of the resulting Me(II)-Al(III)-LDH precipitates using the equilibrium metal concentration values obtained from the long term kinetics.

MATERIALS AND METHODS

Mineral substrate

The sorbent used for the adsorption experiments is γ-Al_2O_3 purchased from Degussa. The purity of this substrate is >99.6% with an average particle size of 13 nm and a BET surface area of 100 ± 15 m^2g^{-1} [2]. Powder X-ray diffraction (XRD) measurements of hydrated γ-Al_2O_3 samples used in our study are shown in Figure 1, and confirm that the γ-Al_2O_3 substrate is metastable and transforms into a mixture of gibbsite and bayerite, as observed in previous studies [2, 26-28].

Batch sorption experiments

The sorption experiments were conducted inside a glovebox with a 95% N_2-5% H_2 atmosphere to exclude $O_{2(g)}$ and $CO_{2(g)}$, in order to prevent redox reactions (of concern for Fe(II) and Mn(II)) and any impacts of dissolved carbonate on metal sorption. The doubly deionized (DDI) water used for sample and reagent preparation was boiled to remove dissolved carbonate and oxygen, and then cooled inside the glovebox. The glovebox air was circulated continuously through granular Palladium catalyst using a fanbox (Coy Laboratories) to eliminate $O_{2(g)}$.

The batch experiments involved kinetic studies monitoring the sorption of dissolved Ni(II), Zn(II), Co(II), Fe(II) and Mn(II) onto γ-Al$_2$O$_3$ over the course of weeks to months to ensure that sorption equilibrium was achieved. The γ-Al$_2$O$_3$ suspension density of the samples was 5.0 g L^{-1}, while ionic strength was set at 0.1M with NaCl, and the metal concentration was 1 or 3 mM. For each metal, experiments were conducted at 3-4 pH values in the near-neutral to alkaline range where formation of Me(II)-Al(III)-LDH occurs under the conditions of this study. Suspension pH values were stabilized by addition of 25 mM of Good's buffers to the background electrolyte. The buffers used were CHES (pKa = 9.30), EPPS (pKa = 8.00), HEPES (pKa = 7.50), and MES (pKa=6.10) to cover the pH 6.5-9.5 range. Each sample was run in duplicate to account for experimental variability.

The suspensions were hydrated for 3 days, and then spiked with appropriate aliquots of anoxic 0.1 M MeCl$_2$ (Me= Ni, Zn, Co, Fe and Mn) to achieve an initial Me(II) concentration of 1.0 mM. For Zn(II), a second set of experiments was conducted employing Zn(II) concentrations of 3 mM. The reaction vessels were kept airtight inside the glovebox and samples were taken regularly over the course of several months. Sampling involved measurement of suspension pH, followed by syringe filtration of a 10 mL subsample through 0.22 μm nitrocellulose membrane into a 15 mL polyethylene tube containing a small aliquot of concentrated HCl. The acidified filtrates were analyzed for the concentration of remaining aqueous Me(II) using flame atom absorption spectrometry (FAAS).

Control suspensions containing 5 g/L γ-Al$_2$O$_3$ hydrated in the same background electrolyte as the sorption samples but without metal added were also analyzed by

powder X-ray diffraction (XRD) to determine the transformation products of γ-Al₂O₃ that control the aqueous Al-solubility in the suspensions. Control suspensions containing γ-Al₂O₃ but no metal added and adjusted to the pH values of the sorption studies, were left hydrated in the glovebox. These controls were then analyzed by powder X-ray diffraction (XRD). Powder samples were loaded on low background sample holders and analyzed by Bruker D8 Advance diffractometer using Ni-filtered Cu Kα radiation and a LynxEye XE detector. The X-ray generator was set to a tube current of 25 mA and a tube voltage of 40 kV. XRD data were collected over the 5-75° 2θ range, with a step size of 0.02° 2θ and a counting time of 2 seconds per step.

XAS analyses

XAS measurements were performed to assess the precipitation of Me(II)-All(III)-LDH phases in our experiments. After macroscopic equilibrium had been reached, reacted Al-oxide solids were collected by filtering 30 mL aliquots taken from the batch kinetic reactors described in the previous section. The solids were sealed into EXAFS samples holders using Kapton tape, and transported under anaerobic conditions to the synchrotron facility as in our previous work [2, 29]. The EXAFS measurements were conducted at beamline 12-BMB of the Advanced Photon Source at Argonne National Laboratory. Scanning was done at the *K*-edges of Ni (8333 eV), Zn (9659 eV), Co (7709 eV), Fe (7112 eV) or Mn (6539 eV). The analyses were performed at room temperature and in fluorescence mode using a Canberra multi-element detector. EXAFS data analysis was performed with WinXAS 3.1[30] in combination with Atoms and Feff[31] using standard procedures[2].

Thermodynamic calculations

We estimated the Ksp values of the Me(II)-Al(III)-LDH phases formed in the equilibrated Me(II)-γAl$_2$O$_3$ samples (where Me= Ni, Zn, Co, Fe or Mn) using the method of Zhu and Elzinga[29]. This approach assumes that Me(II)-Al(III)-LDH phases control the Me(II) solubility in the sorption samples, so that Ksp can be calculated from the concentration of aqueous Me(II) in the equilibrated suspensions[29]. The systems for which these calculations were performed were selected based on two criteria: (1) Me(II)-Al(III)-LDH had formed in the equilibrated suspensions, as determined by the XAS analyses; and (2) the concentration of dissolved metal in the equilibrated solutions was sufficiently high for reliable analysis by FAAS. The calculations assumed that the secondary Me(II)-Al(III)-LDH phases take on the ideal structural Me(II):Al(III) molar ratio of 2:1, so that their chemical formula is Me(II)$_{2/3}$Al(III)$_{1/3}$(OH)$_2$Cl$_{1/3}$. The aqueous chemical equilibrium of these phases can be expressed as:

$$\text{Me(II)}_{2/3}\text{Al(III)}_{1/3}\text{(OH)}_2\text{Cl}_{1/3\,(s)} \leftrightarrow \frac{2}{3}\,\text{Me}^{2+} + \frac{1}{3}\,\text{Al}^{3+} + 2\,\text{OH}^- + \frac{1}{3}\,\text{Cl}^- \qquad (1)$$
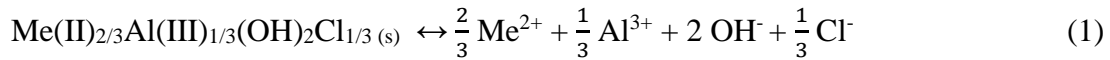
The corresponding solubility product Ksp is:

$$\text{Ksp} = (\text{Me}^{2+})^{2/3} \times (\text{Al}^{3+})^{1/3} \times (\text{OH}^-)^2 \times (\text{Cl}^-)^{1/3} \qquad (2)$$

where round brackets denote ion activities. In our experiments, the aqueous OH$^-$ activities were determined from the equilibrium pH values, while the equilibrium Me$^{2+}_{(aq)}$ concentrations were measured, and the Cl$^-_{(aq)}$ concentration was set by the background electrolyte. The concentration of dissolved Al^{3+}, however, was too low for detection by our analytical techniques. Therefore, (Al^{3+}) was calculated by assuming that the solutions were in equilibrium with either gibbsite (α-Al(OH)$_3$) or bayerite (β-Al(OH)$_3$), which are the Al-oxide phases formed during transformation of the γ-Al$_2$O$_3$ sorbent in our systems

as determined by XRD analyses of the Al-oxide solids (Figure 1). Activity coefficients for converting concentrations into activities were calculated with the Davies equation, while free aqueous metal activities were determined by accounting for aqueous complexation of dissolved Me^{2+} with aqueous Cl^- and OH^-. The activity and aqueous complexation corrections were calculated with the program Visual MINTEQ version 3.0 and the associated thermodynamic database.

In a second set of calculations, Ksp was determined according to:

$$Ksp = (Me^{2+})^{2/3} \times (Al^{3+})^{1/3} \times (OH^-)^2 \tag{3}$$

This approach was based on Regelink and Temminghoff[25] who suggested that the formation of LDH phases may be unaffected by the concentration of the interlayer anion (here Cl^-) when the anion is present in excess relative to the concentrations of Me(II) and Al(III). Accordingly, the anion activity is excluded from the calculation of solubility product values.

RESULTS AND DISCUSSION

Batch Kinetic Results

The results of the batch kinetic studies are presented in Figure 2, which plots the aqueous metal concentrations as a function of time at the various pH values investigated for each metal. As perhaps expected, there are differences in sorption behavior between the metals, but some general similarities are observed as well. All systems exhibit biphasic metal sorption kinetics, where an initial fast sorption step within the first 1-2 days of reaction is followed by a slow reaction stage that continues until equilibrium is reached (Figure 2). Equilibration is slow in these systems, with reaction times on the order of

weeks to months required to achieve sorption equilibrium (Figure 2). Suspension pH has

a distinct impact on the kinetic sorption patterns, with both the extent and the rate of

metal sorption increasing with pH (Figure 2). For example, Fe(II) sorption equilibrium is

reached after approximately 21, 64 and 104 days at pH 8.0, 7.5 and 7.0, respectively, with

corresponding removal of ~95%, 75% and 20% of added Fe(II)$_{aq}$ (Figure 2e). A similar

pH effect is observed for the other metals. Of note are the distinct differences between the

five metals with respect to the affinity of sorption at a given pH value. As an example, at

pH 7.5, we observe removal (i.e. sorption) of 90% of added Ni(II) but of only 10% of

added Fe(II) (Figure 2a versus 2e). We interpret these differences in sorption affinity to

reflect metal-dependent differences in the stability and solubility of the secondary Me(II)-

Al(III)-LDH sorption products formed, as discussed below.

XAS Data

The extended X-ray adsorption fine structure (EXAFS) data of selected sorption samples

are presented in Figure 3, with Figure 3a showing the raw and fitted k^3-weighted χ

spectra, and Figure 3b the corresponding radial structure functions (RSFs) obtained from

Fourier transformation of the raw χ data. The EXAFS data fitting results are summarized

in Table 1.

The RSFs shown in Figure 3b all contain two peaks. The first is observed at R+ΔR ~1.8

Å and represents the first-shell O ligands surrounding the central Me(II) cation. The

second shells at R+ΔR ~2.9 Å are due to the presence of metal neighbors in the

coordination environment of the metal sorbates, and indicate the formation of secondary

metal precipitates in these samples. Fits of the first shells yield coordination numbers of

5.3-6.4 for the O atomic neighbors (Table 1), consistent with an octahedral arrangement

of the first-shell O ligands around central Me(II). The corresponding radial distances increase from 2.05 Å for Ni and Zn, to 2.08 Å for Co(II), 2.11 Å for Fe(II) , and 2.16 Å for Mn(II). These values are consistent with the results of previous EXAFS studies of the sorption products formed by these metals [2, 6, 8, 14, 15, 21, 29, 32-34], and confirm the octahedral Me-O coordination suggested by the fitted coordination numbers of the first shells[35]. The gradual decrease in Me-O separation with atomic number reflects the contraction in atomic radius for elements along each row of the periodic table, attributed to increased nuclear charge.

Fits of the second shells accounted for mixed contributions of second-neighbor Me(II) and Al(III) scatterers. Although good fits were obtained when accounting for only second-neighbor Me(II) contributions, second-shell Al(III) was included as well. This was done because the raw k^3-weighted χ spectra of the sorption samples strongly resemble the spectra of the Me(II)-Al(III)-LDH phases that can be confirmed from previous studies[2, 3, 8, 15, 18]. A key diagnostic feature is the truncated oscillation at 7-8 Å^{-1} (circled in Figure 3a) which is observed in all sorption spectra and has been proposed as a fingerprint to distinguish Me(II)-Al(III)-LDH precipitates from α- and β-Me(II)(OH)$_2$ and Me(II)-phyllosilicate phases[6]. Because of the presence of Me(II)-Al(III)-LDH in these samples, the second shells were fitted assuming the presence of both Me(II) and Al(III) metal neighbors. The corresponding radial distances increase from 3.05 Å for Ni(II), to 3.08 Å for Zn(II) and Co(II), to 3.13 Å for Fe(II) and 3.19 Å for Mn(II) (Table 1). These values are consistent with the values of previous EXAFS studies of the Me(II)-Al(III)-LDH phases formed by these metals [2, 6, 8, 14, 15, 21, 29, 32-34], and indicate expansion of the LDH lattice with increasing ionic radius of the structural Me(II) cation. The EXAFS

results (Figure 3) confirm that the five metals studied here form secondary Me(II)-Al(III)-LDH phases during sorption onto Al-oxide at near neutral to alkaline pH.

For Zn(II), the LDH features are weak in the EXAFS data of the sorption samples prepared at the 1mM used for the sorption studies (Figure 4), and the first-shell Zn-O distance is shorter than would be expected for octrahedral Zn(II) in Zn(II)-Al(III)-LDH. We attribute this to the presence of a substantial population of monomeric Zn(II) complexes with a tetrahedral Zn-O coordination, which form in addition to Zn(II)-Al(III)-LDH, as also observed by Li et al.[33]. A second set of experiments was conducted using a Zn(II) concentration of 3 mM. EXAFS analysis shows that these 3 mM samples are dominated by Zn(II)-Al(III)-LDH, as evidenced by the Zn-O distance of 2.06 indicative of octahedral Zn(II) (Table 1). The Zn(II)-Al(III)-LDH solubility products estimated for the 1mM and 3mM samples are similar (Table 2). This suggests that Zn(II)-Al(III)-LDH controls Zn(II) solubility in the lower concentration samples as well, and that the stability of the Zn(II)-Al(III)-LDH phases formed in the high and low concentration systems is similar.

Ksp Estimates

Table 2 represents the detailed ion concentrations, activities and calculation results of Ksp for the Me(II)-Al(III)-LDH phases formed in the Me(II)-γAl$_2$O$_3$ sorption systems (Me = Ni, Zn, Co, Fe, Mn) and Table 3 summarizes the average Ksp values (with associated uncertainties) of these metals . The values reported in Table 3 include those calculated with and without account of anion (Cl-) activity, and assuming either gibbsite or bayerite as the Al-oxide mineral phase controlling Al solubility. The Ksp values of the

β-Me(II)(OH)$_2$ phases formed by the five metals and the Ksp values measured in previous studies, are listed as well in Table 3.

Comparisons between the average Ksp values of Me(II)-Al(III)-LDH phases show that Ni(II)-Al(III)-LDH has the lowest solubility (average Ksp = 8.43 (±0.01) × 10^{-23}) whereas Mn(II)-Al(III)-LDH is the most soluble (average Ksp = 1.28 (±0.02) × 10^{-20}). This range in Ksp value translates into a 3-order magnitude difference in dissolved Ni(II) versus dissolved Mn(II) at given pH, and thus indicates substantial variation in the stability and thermodynamic favorability of Me(II)-Al(III)-LDH precipitation among the five metals considered in this study. This is reflected in the macroscopic data, where notable differences in the extent of metal sorption are observed at a given pH value (Figure 2).

The average solubility (Ksp) values are accompanied by uncertainties that are calculated from the Ksp estimates at the different pH values studied for each metal (Table 3). These uncertainties range from approximately 0.1% of the average for Ni(II) to 5.8% for Co(II), while those of Zn(II), Mn(II) and Fe(II) are 2.5%, 1.7% and 0.8%, respectively. Although overall small, these uncertainties are larger than the variations within the replicate series run for each pH value, which mostly are < 0.1 %. This suggests that factors beyond random experimental error contribute to the uncertainties in Ksp as well. One such factor is the availability of dissolved Al in these systems, which is controlled by the solubility of the Al-oxide substrate. The γ-Al$_2$O$_3$ sorbent is metastable and converts into a mixture of bayerite (β-Al(OH)$_3$) and gibbsite (α-Al(OH)$_3$) (Figure 1). Solution pH has a distinct impact on the transformation process, with an increasing proportion of bayerite (relative to gibbsite) formed at higher pH (Figure1)[26-28]. This pH

effect on γ-Al_2O_3 transformation may affect the calculation of Ksp, because bayerite has a higher Al-solubility (least thermodynamically stable phase of aluminum hydroxide) than gibbsite[27, 36, 37] (Table 2). Thus, while the calculations of Ksp in the current study assume a single Al-oxide phase controlling the dissolved Al^{3+} activity (Table 2), the actual activity is in fact controlled by a mixture of Al-oxide phases that change proportion with pH. This may lead to pH-dependent differences in the estimated Ksp values, generating uncertainty in the calculations. An additional factor may be the interaction of metal cations with the Al-oxide surface, which may lead to the formation of inner-sphere surface complexes through adsorption. The adsorption of metal cations at the Al-oxide may block reactive sites and thereby hinder Al dissolution, as observed for the Fe(III)-oxides [38, 39]. This effect would vary with pH, as metal adsorption is pH-dependent.[27] Another potential factor is the pH dependence of the LDH precipitation rate (Figure 2). This may lead to differences in the particle size and composition of the LDH phases formed at lower versus higher pH, causing differences in their solubilities. It is plausible that these and perhaps other factors combine to generate uncertainty in Ksp beyond random error. Despite these variations, however, we note that the uncertainties in Ksp for individual metals are much smaller than the differences in Ksp values between the five metals (Table 2). We therefore conclude that our results are robust with respect to defining the relative differences in solubility of the LDH phases formed by these metals.

Now if we inspect the data reported in Table 3, it suggests that the Ksp values of Me(II)-Al(III)-LDH and β-Me(II)(OH)$_2$ are correlated. To be consistent, solubility product values of the metal hydroxide phases reported in the Visual MINTEQ database were recalculated in accordance with the equation used to calculate the Ksp values of the

corresponding LDH phases. Visual MINTEQ provides the solubility product values of crystalline β-Me(II)(OH)$_2$ phases using the equilibrium equation written below :

$$Me(OH)_{2(c)} + 2H^+ \leftrightarrow Me^{2+} + 2H_2O \tag{4}$$

Thus we added the water equilibrium equation $H_2O \leftrightarrow H^+ + OH^-$, log Kw = -14 (where Kw is the solubility product of water) to rearrange the Visual MINTEQ equation as:

$$Me(OH)_{2(c)} \leftrightarrow Me^{2+} + 2OH^- \tag{5}$$

Figure 5 plots the log-transformed Ksp values of Me(II)-Al(III)-LDH (calculated with equation 1 assuming that (Al^{3+}) is controlled by gibbsite) against those of β-Me(II)(OH)$_2$, and reveals a linear relation between the two parameters. This is notable that the solubility of the Me(II)-Al(III)-LDH phases considered here is not affected in a major way by the size mismatch between Al(III) and the Me(II) cations. There is a pronounced difference in size between the Al(III) cations that substitute into the brucitic β-Me(II)(OH)$_2$ sheets to form Me(II)-Al(III)-LDH. This likely imposes a structural "penalty" that partially offsets the overall higher stability of Me(II)-Al(III)-LDH relative to β-Me(II)(OH)$_2$. This effect is expected to become increasingly pronounced as the relative size of Me(II) to Al(III) increases [24], yielding a non-linear relation between the Ksp values of β-Me(II)OH)$_2$ and Me(II)-Al(III)-LDH. Since we instead observe a linear relation between the two Ksp values (Figure 5), we conclude that the effect is small relative to the difference in stability of the β-Me(II)(OH)$_2$ basis structures. As a result, the solubility of the Me(II)-Al(III)-LDH phases studied here can be predicted in a rather robust fashion from the Ksp values of the corresponding Me(OH)$_2$ phases.

A final comparison we make for the data presented in Table 3 is that of the Ksp

values determined in the current study to those reported for Ni(II), Zn(II), Co(II) and

Fe(II) reported in earlier studies [9, 18, 25]. Ksp values provided by different other studies

were recalculated to the same chemical equilibrium expression used in our study

(Equation 2). This was done by adjusting the stoichiometry of the components and adding

the water equilibrium to set up the provided thermodynamic equilibriums to produce the

equation used in current study. As an example, the equation used by Peltier et al.[18] was:

$$\text{Ksp}_{\text{(initial 1)}} = ((Me^{2+})^x (Al^{3+})^{(1-x)} (A^{n-})^{(1-x)/n}) / (H^+)^2 \tag{6}$$

Where Ksp $_{\text{(initial 1)}}$ is the Ksp value provided by Peltier et al.[18] and x= 0.67. Thus we

recalculated the provided solubility product values based on the stoichiometry of the

equation used in the current work and found the relation Ksp $_{\text{(final 1)}}$ = Ksp $_{\text{(initial 1)}}$ × 10^{-28}

where Ksp $_{\text{(final 1)}}$ is the converted solubility product value. Similarly the solubility product

values provided by Regelink and Temminghoff[25] and Johnson and Glasser[9] were

converted using the relation Ksp $_{\text{(final 2)}}$ = (Ksp $_{\text{(initial 2)}}$)$^{1/3}$ × 10^{-28}. Where Ksp $_{\text{(initial 2)}}$ and

Ksp $_{\text{(final 2)}}$ are the provided and the converted solubility product values respectively. Both

of these studies used the same equation for their solubility product (Ksp $_{\text{(initial 2)}}$)

calculations which can be written as:

$$\text{Ksp}_{\text{(initial 2)}} = ((Me^{2+})^2 (Al^{3+}) (A^{n-})^{1/n}) / (H^+)^6 \tag{7}$$

Hence, these converted Ksp values were used to compare with the Ksp values obtained

from the current study. A global comparison indicates that our values are within an order

of magnitude of those reported by Johnson and Glasser[9] and Regelink and

Temminghoff[25], while the differences with the values of Peltier et al.[18] are larger,

amounting to approximately two orders of magnitude (Table 3). Peltier et al.[18] estimated the solubility of Ni(II)-Al(III)-LDH as 1.58×10^{-24} which is much lower than the values reported by Regelink and Temminghoff[25] or Johnson and Glasser[9] as well as the current study. We have a similar estimate (calculation done considering the presence of gibbsite) to Regelink and Temminghoff[25] for the Ni(II)-Al(III)-LDH phase when the anion activity is present in the calculation but the estimates differ when the calculations were done without anion activity. For both Co(II)- and Zn(II)-Al(III)-LDH phases, most the estimates from our work are lower than the values reported by Johnson and Glasser[9].

There are many factors that may contribute to these discrepancies, including differences in sample preparation, LDH composition, and the method of Ksp estimation. All these other studies used CO_3^{2-} interlayered LDH whereas our work used Cl^- as the interlayer anion which has obvious impact on the stability of the resulting phase and hence can lead to a different solubility value as already proved[40]. Also the solubility of the LDH phases can be different based on the method used, which is apparent from the above mentioned values. Peltier et al.[18] used a more direct method using the enthalpy of formation to calculate solubility for Ni(II)-Al(III)-LDH where they used dry samples for the measurements which can have a significant impact on the resulting solubility measurements. Regelink and Temminghoff[25] determined the solubility product values based on solubility measurements which was also used by Johnson and Glasser[9]. Also the LDH substrates they used for Ksp measurements were synthesized by directly mixing the separate Me(II) solutions with Al(III) solutions in a basic environment which is very different from the LDH producing environment used in our study. These differences can

lead to difference in thermodynamic properties of formed LDH phases like particle size, composition and morphology which can affect the overall stability of the LDH phases.

Regelink and Temminghoff[25] demonstrated that the difference in the solubility value between them and Johnson and Glasser[9] may come from the higher CO_3^{2-} concentration used by the later. Regelink and Temminghoff[25] also stated that the change of Ni:Al ratio may not affect the predicted Ni solubility as a function of pH but it can affect the absolute value of the calculated solubility product. We used long term sorption equilibriums to calculate the solubility values, where the Me:Al ratio may or may not reach the ideal 2:1 ratio and thus can evidently affect the solubility estimates. Al availability is the key factor to control solubility in this type of long term metal sorption studies. Zhu and Elzinga[29] determined the solubility of Fe(II)-Al(III)-LDH as $1.21(\pm0.0416)\times10^{-21}$ and $2.41(\pm0.0721)\times10^{-21}$ (considering the presence of gibbsite and bayerite respectively) during the long term Fe(II) sorption onto γ-Al_2O_3. We obtained slightly lower values for the same phase where the difference may arise from the use of a different starting adsorbent γ-Al_2O_3. Although the value reported by Zhu and Elzinga[29] is different from the value determined in the current study but that aptly fits in Figure 5 thus gives a good correlation.

The removal of aqueous Me(II) in our systems most likely involves a combination of two different mechanisms: (1) the adsorption of Me(II) onto the surface of the aluminum oxide adsorbent, and (2) the precipitation of secondary Me(II)-Al(III)-LDH phases. The existence of these two different metal species are evident in the 1 mM Zn(II) system, where adsorbed and precipitated species can be distinguished using EXAFS because of their different oxygen coordination (tetrahedral versus octahedral for adsorbed

and precipitated Zn(II), respectively).[33] While it is likely that they occur for the other metals as well, the octahedral coordination of both adsorbed and precipitated Ni(II), Co(II), Mn(II) and Fe(II) makes their distinction problematic based on EXAFS. The question whether the processes metal adsorption and precipitation are related mechanistically (e.g. adsorption transitions to precipitation) cannot be determined from our data. However, the results of the Zn(II) systems demonstrate that the adsorbed and precipitated metal complexes co-exist as separate species under equilibrium conditions, and can therefore be accounted for individually in geochemical models.

ENVIRONMENTAL IMPLICATIONS

The thermodynamic data acquired here indicate substantial differences in the propensity of Me(II)-Al(III)-LDH formation, with Ni(II) having the highest favorability for forming LDH phases, and Mn(II) the lowest. It is interesting to note that the studies that have identified Me(II)-Al(III)-LDH minerals in natural samples involved Ni(II) and Zn(II) [18, 19, 21, 23], which are the two metals most likely to form LDH phases based on our thermodynamic data (Figure 5).

We used our thermodynamic dataset to understand the potential importance of Me(II)-Al(III)-LDH precipitation in a model groundwater system characterized in (Table 4) [41], and in a calcitic system. In both systems we assumed an atmospheric CO_2 partial pressure. The solubility products of the five Me(II)-Al(III)-LDH phases (calculated considering the concentration of Cl^- in the calculation of Ksp, and gibbsite as the aluminum controlling phase) were incorporated into the database of Visual MINTEQ 3.0 to calculate the dissolved metal concentrations over the pH range 6.0-10.0. The results of

these calculations were compared with the estimates obtained under similar environmental conditions but using $Me(OH)_2$s and $MeCO_3$ as the dissolved metal controlling phases. The results are presented in Figures 6 (groundwater system) and 7 (calcitic system). For all the five metals, $MeCO_3$ emerged as the least soluble (i.e. most stable) phase in both environments, while $Me(OH)_2$ was the most soluble, and $Me(II)$-$Al(III)$-LDH was intermediate. The exception is $Ni(II)$ and $Zn(II)$ in the calcitic system, where LDH emerged as the least soluble phase (Figure 7). Overall, these results suggest that metal carbonates are the main control on metal solubility in these environments. However, factors other than thermodynamic favorability need to be considered for predicting the formation of secondary metal phases in natural environment. Strongly sorbing compounds like humic acids and phosphate anions may interfere with the formation of pure $MeCO_{3(s)}$ by adsorption onto nucleation sites poisoning precipitate growth [42](e.g. Kirk, 1997). These compounds may hinder formation of $MeCO_{3(s)}$ natural systems such as soils even when substantial supersaturation occurs. In contrast, LDH phases have been shown to form in soil environments [22, 43], suggesting that the formation of these minerals is not particularly susceptible to interference by foreign solutes. A further consideration is that the $Me(II)$-$Al(III)$-LDH phases characterized in this study contain Cl^- as the interlayer anion. Peltier et al.[18] have demonstrated that the identity of the interlayer anion has a substantial impact on the stability of the $Me(II)$-$Al(III)$-LDH, with carbonate anions providing the most stability, yielding lower Ksp values. Application of the Ksp values of the chloride-interlayered LDH phases determined here underpredict the presence of LDHs in natural environments, where CO_3^{2-} likely is the

prevalent interlayer anion. Further thermodynamic and field-based studies are needed to investigate the formation and stability of Me(II)-Al(III)-LDH phases in natural systems.

REFERENCES

1. Elzinga, E. J.; Sparks, D. L., Phosphate adsorption onto hematite: an in situ ATR-FTIR investigation of the effects of pH and loading level on the mode of phosphate surface complexation. *J. Colloid Interface Sci.* **2007,** *308*, (1), 53-70.

2. Elzinga, E. J., Formation of Layered Fe(II)–Al(III)-Hydroxides during Reaction of Fe(II) with Aluminum Oxide. *Environmental science & technology* **2012,** *46*, (9), 4894-4901.

3. Scheidegger, A. M.; Strawn, D. G.; Lamble, G. M.; Sparks, D. L., The kinetics of mixed Ni-Al hydroxide formation on clay and aluminum oxide minerals: a time-resolved XAFS study. *Geochimica et Cosmochimica Acta* **1998,** *62*, (13), 2233-2245.

4. O'Day, P. A.; Rehr, J. J.; Zabinsky, S. I.; Brown, G. E., Jr., Extended X-ray Absorption Fine Structure (EXAFS) Analysis of Disorder and Multiple-Scattering in Complex Crystalline Solids. *J. Am. Chem. Soc.* **1994,** *116*, (7), 2938-2949.

5. Scheckel, K. G.; Sparks, D. L., Kinetics of the Formation and Dissolution of Ni Precipitates in a Gibbsite/Amorphous Silica Mixture. *J. Colloid Interface Sci.* **2000,** *229*, (1), 222-229.

6. Scheinost, A. C.; Sparks, D. L., Formation of Layered Single- and Double-Metal Hydroxide Precipitates at the Mineral/Water Interface: A Multiple-Scattering XAFS Analysis. *J. Colloid Interface Sci.* **2000,** *223*, (2), 167-178.

7. Scheidegger, A. M.; Sparks, D. L.; Fendorf, M., Mechanisms of Nickel Sorption on Pyrophyllite: Macroscopic and Microscopic Approaches. *Soil Sci. Soc. Am. J.* **1996,** *60*, (6), 1763-1772.

8. Scheidegger, A. M.; Lamble, G. M.; Sparks, D. L., Spectroscopic Evidence for the Formation of Mixed-Cation Hydroxide Phases upon Metal Sorption on Clays and Aluminum Oxides. *J. Colloid Interface Sci.* **1997,** *186*, (1), 118-128.

9. Johnson, C. A.; Glasser, F. P., Hydrotalcite-like minerals ($M_2Al(OH)_6(CO_3)_{0.5}.XH_2O$, where M = Mg, Zn, Co, Ni) in the environment: synthesis, characterization and thermodynamic stability. *Clays and Clay Minerals* **2003,** *51*, (1), 1-8.

10. Elzinga, E. J.; Sparks, D. L., Nickel Sorption Mechanisms in a Pyrophyllite–Montmorillonite Mixture. *J. Colloid Interface Sci.* **1999,** *213*, (2), 506-512.

11. Roberts, D. R.; Scheidegger, A. M.; Sparks, D. L., Kinetics of Mixed Ni−Al Precipitate Formation on a Soil Clay Fraction. *Environmental science & technology* **1999,** *33*, (21), 3749-3754.

12. Roberts, D. R.; Ford, R. G.; Sparks, D. L., Kinetics and mechanisms of Zn complexation on metal oxides using EXAFS spectroscopy. *J. Colloid Interface Sci.* **2003,** *263*, (2), 364-376.

13. Scheidegger, A. M.; Sparks, D. L., Kinetics of the formation and the dissolution of nickel surface precipitates on pyrophyllite. *Chemical Geology* **1996,** *132*, (1–4), 157-164.

14. Thompson, H. A.; Parks, G. A.; Brown, G. E., Dynamic interactions of dissolution, surface adsorption, and precipitation in an aging cobalt (II)-clay-water system. *Geochimica et Cosmochimica Acta* **1999,** *63*, (11), 1767-1779.

15. Ford, R. G.; Sparks, D. L., The Nature of Zn Precipitates Formed in the Presence of Pyrophyllite. *Environmental science & technology* **2000,** *34*, (12), 2479-2483.

16. Towle, S. N.; Bargar, J. R.; Brown Jr, G. E.; Parks, G. A., Surface Precipitation of Co(II)(aq) on Al2O3. *J. Colloid Interface Sci.* **1997,** *187*, (1), 62-82.

17. Elzinga, E. J.; Sparks, D., Reaction condition effects on nickel sorption mechanisms in illite–water suspensions. *Soil Science Society of America Journal* **2001,** *65*, (1), 94-101.

18. Peltier, E.; Allada, R.; Navrotsky, A.; Sparks, D. L., Nickel solubility and precipitation in soils: a thermodynamic study. *Clays and Clay Minerals* **2006,** *54*, (2), 153-164.

19. Peltier, E.; Lelie, D. v. d.; Sparks, D. L., Formation and Stability of Ni−Al Hydroxide Phases in Soils. *Environmental science & technology* **2010,** *44*, (1), 302-308.

20. McNear, D. H.; Chaney, R. L.; Sparks, D. L., The effects of soil type and chemical treatment on nickel speciation in refinery enriched soils: A multi-technique investigation. *Geochimica et Cosmochimica Acta* **2007,** *71*, (9), 2190-2208.

21. Voegelin, A.; Kretzschmar, R., Formation and dissolution of single and mixed Zn and Ni precipitates in soil: Evidence from column experiments and extended X-ray absorption fine structure spectroscopy. *Environmental science & technology* **2005,** *39*, (14), 5311-5318.

22. Nachtegaal, M.; Sparks, D. L., Nickel sequestration in a kaolinite-humic acid complex. *Environmental science & technology* **2003,** *37*, (3), 529-534.

23. Jacquat, O.; Voegelin, A.; Villard, A.; Marcus, M. A.; Kretzschmar, R., Formation of Zn-rich phyllosilicate, Zn-layered double hydroxide and hydrozincite in contaminated calcareous soils. *Geochimica et Cosmochimica Acta* **2008,** *72*, (20), 5037-5054.

24. Allada, R. K.; Peltier, E.; Navrotsky, A.; Casey, W. H.; Johnson, C. A.; Berbeco, H. T.; Sparks, D. L., Calorimetric determination of the enthalpies of formation of

hydrotalcite-like solids and their use in the geochemical modeling of metals in natural waters. *Clays and Clay Minerals* **2006,** *54*, (4), 409-417.

25. Regelink, I. C.; Temminghoff, E. J. M., Ni adsorption and Ni–Al LDH precipitation in a sandy aquifer: An experimental and mechanistic modeling study. *Environmental Pollution* **2011,** *159*, (3), 716-721.

26. Wijnja, H.; Schulthess, C., ATR–FTIR and DRIFT spectroscopy of carbonate species at the aged γ-Al 2 O 3/water interface. *Spectrochimica Acta Part A: Molecular and Biomolecular Spectroscopy* **1999,** *55*, (4), 861-872.

27. Carrier, X.; Marceau, E.; Lambert, J.-F.; Che, M., Transformations of γ-alumina in aqueous suspensions: 1. Alumina chemical weathering studied as a function of pH. *J. Colloid Interface Sci.* **2007,** *308*, (2), 429-437.

28. Tang, Y.; Reeder, R. J., Uranyl and arsenate cosorption on aluminum oxide surface. *Geochimica et Cosmochimica Acta* **2009,** *73*, (10), 2727-2743.

29. Zhu, Y.; Elzinga, E. J., Formation of Layered Fe(II)-Hydroxides during Fe(II) Sorption onto Clay and Metal-Oxide Substrates. *Environmental science & technology* **2014,** *48*, (9), 4937-4945.

30. Ressler, T., WinXAS: A new software package not only for the analysis of energy-dispersive XAS data. *Le Journal de Physique IV* **1997,** *7*, (C2), C2-269-C2-270.

31. Ankudinov, A. L.; Rehr, J., Relativistic calculations of spin-dependent X-ray-absorption spectra. *Physical Review B* **1997,** *56*, (4), R1712.

32. Scheckel, K. G.; Scheinost, A. C.; Ford, R. G.; Sparks, D. L., Stability of layered Ni hydroxide surface precipitates—a dissolution kinetics study. *Geochimica et Cosmochimica Acta* **2000,** *64*, (16), 2727-2735.

33. Li, W.; Livi, K. J. T.; Xu, W.; Siebecker, M. G.; Wang, Y.; Phillips, B. L.; Sparks, D. L., Formation of Crystalline Zn–Al Layered Double Hydroxide Precipitates on γ-Alumina: The Role of Mineral Dissolution. *Environmental science & technology* **2012,** *46*, (21), 11670-11677.

34. Thompson, H. A.; Parks, G. A.; Brown, G. E., Formation and release of cobalt (II) sorption and precipitation products in aging kaolinite–water slurries. *J. Colloid Interface Sci.* **2000,** *222*, (2), 241-253.

35. Shannon, R. D., Revised effective ionic radii and systematic studies of interatomic distances in halides and chalcogenides. *Acta crystallographica section A: crystal physics, diffraction, theoretical and general crystallography* **1976,** *32*, (5), 751-767.

36. Parks, G. A., Free energies of formation and aqueous solubilities of aluminum hydroxides and oxide hydroxides at 25 C. *Amer. Mineral.* **1972,** *57*, (7), 1163-1189.

37. Demichelis, R.; Civalleri, B.; Noel, Y.; Meyer, A.; Dovesi, R., Structure and stability of aluminium trihydroxides bayerite and gibbsite: A quantum mechanical ab initio study with the Crystal06 code. *Chemical Physics Letters* **2008,** *465*, (4–6), 220-225.

38. Giovanoli, R.; Cornell, R. M., Crystallization of metal substituted ferrihydrites. *Journal of Plant Nutrition and Soil Science* **1992,** *155*, (5), 455-460.

39. Ford, R. G.; Bertsch, P. M.; Farley, K. J., Changes in transition and heavy metal partitioning during hydrous iron oxide aging. *Environmental science & technology* **1997,** *31*, (7), 2028-2033.

40. Kumar Allada, R.; Navrotsky, A.; Berbeco, H. T.; Casey, W. H., Thermochemistry and aqueous solubilities of hydrotalcite-like solids. *Science* **2002,** *296*, (5568), 721-723.

41. Tang, J.; Johannesson, K. H., Speciation of rare earth elements in natural terrestrial waters: assessing the role of dissolved organic matter from the modeling approach. *Geochimica et Cosmochimica Acta* **2003,** *67*, (13), 2321-2339.

42. Kirk, G., *The Biogeochemistry of Submerged Soils*. John Wiley & Sons, Ltd: Chichester, 2004; p 282.

43. Zhu, Y.; Liu, J.; Elzinga, E. J., Effect of organic compounds on Fe (II) sorption onto clay and aluminum oxide minerals. *Abstracts of Papers of The American Chemical Society* **2014**, 248; Amer Chemical Soc 1155 16th St, NW, WASHINGTON, DC 20036 USA: 2014.

Appendix A: Tables

Table 1. Me(II) K-Edge EXAFS Fitting Results of Me(II)-γAl_2O_3(Me=Ni, Zn, Co, Fe, Mn) sorption samples.

					Atomic shell [a]					
			Me-O			Me-Me			Me-Al	
Me	P^H	N	R(Å)	σ^2(Å^{-2})	N	R(Å)	σ^2(Å^{-2})	N	R(Å)	σ^2(Å^{-2})
Ni	6.75	5.3	2.05	0.007	3.0	3.05	0.009	3.0	3.05	0.009
	7.00	5.5	2.05	0.007	3.0	3.05	0.009	3.0	3.05	0.009
Zn	7.00	5.7	2.06	0.010	3.0	3.08	0.009	3.0	3.08	0.009
	7.25	6.3	2.05	0.010	3.0	3.08	0.008	3.0	3.08	0.008
	7.50	5.4	2.06	0.009	3.0	3.09	0.009	3.0	3.09	0.009
Co	7.25	6.4	2.08	0.008	3.0	3.09	0.010	3.0	3.09	0.010
	7.50	5.4	2.08	0.007	3.0	3.08	0.009	3.0	3.08	0.009
	7.75	6.3	2.07	0.009	3.0	3.07	0.008	3.0	3.07	0.008
Fe	7.50	5.3	2.11	0.010	3.0	3.13	0.010	3.0	3.13	0.010
	8.00	6.0	2.11	0.010	3.0	3.12	0.010	3.0	3.12	0.010
Mn	8.75	5.3	2.17	0.010	3.0	3.19	0.010	3.0	3.19	0.010
	9.00	5.4	2.16	0.008	3.0	3.19	0.010	3.0	3.19	0.010
	9.25	5.6	2.16	0.009	3.0	3.20	0.009	3.0	3.20	0.009

[a] N is coordination number, R is interatomic radial distance, and σ^2 is Debye-Weller factor.

Table 2. Ion concentrations, activities and calculation results of Ksp for the Me(II)-Al(III)-LDH phases formed in the Me(II)-γAl_2O_3 sorption systems (Me= Ni, Zn, Co, Fe, Mn) (*Table 2 contd. in pg 26*)

Calculation Results [a]	Ni		Zn						Co			Fe		Mn		
pH	6.75	7.00	7.00 (1mM)	7.25 (1mM)	7.50 (1mM)	7.00 (3mM)	7.25 (3mM)	7.50 (3mM)	7.25	7.50	7.75	7.50	8.00	8.75	9.00	9.25
[Me(II)$_{tot}$] (mol/L)	9.51* 10^{-5}	4.19* 10^{-5}	2.11* 10^{-4}	7.46* 10^{-5}	3.02* 10^{-5}	7.05* 10^{-4}	2.16* 10^{-4}	8.78* 10^{-5}	2.32* 10^{-4}	9.05* 10^{-5}	3.56* 10^{-5}	2.58* 10^{-4}	4.39* 10^{-5}	2.59* 10^{-4}	1.33* 10^{-4}	4.10* 10^{-5}
[Me^{2+}] (mol/L)	9.38* 10^{-5}	4.13* 10^{-5}	1.90* 10^{-4}	6.69* 10^{-5}	2.69* 10^{-5}	6.35* 10^{-4}	1.94* 10^{-4}	7.88* 10^{-5}	2.28* 10^{-4}	8.90* 10^{-5}	3.49* 10^{-5}	2.51* 10^{-4}	4.24* 10^{-5}	2.47* 10^{-4}	1.26* 10^{-4}	3.74* 10^{-5}
[MeCl$^+$] (mol/L)	1.20* 10^{-6}	5.50* 10^{-7}	1.96* 10^{-5}	6.84* 10^{-6}	2.73* 10^{-6}	6.52* 10^{-5}	1.98* 10^{-5}	7.98* 10^{-6}	3.61* 10^{-6}	1.40* 10^{-6}	5.43* 10^{-7}	5.56* 10^{-6}	9.39* 10^{-7}	8.86* 10^{-6}	4.49* 10^{-6}	1.32* 10^{-6}
pH [b] (equilibrium)	6.70	6.93	6.84	7.15	7.39	6.50	6.83	7.09	7.08	7.36	7.59	7.37	7.88	8.59	8.79	9.13
[Cl$^-$] (mol/L) [c]	0.097	0.097	0.097	0.097	0.097	0.097	0.097	0.097	0.097	0.097	0.097	0.097	0.097	0.097	0.097	0.097
[Na$^+$] (mol/L)[d]	0.116	0.103	0.103	0.106	0.109	0.103	0.106	0.109	0.106	0.109	0.113	0.109	0.109	0.101	0.103	0.106
Ionic strength	0.1166	0.1030	0.1033	0.1060	0.1093	0.1042	0.1062	0.1094	0.1063	0.1094	0.1127	0.1097	0.1093	0.1014	0.1033	0.1061
Activity coefficient (γ) for univalent ions	0.77	0.78	0.78	0.78	0.78	0.78	0.78	0.78	0.78	0.78	0.77	0.78	0.78	0.78	0.78	0.78

25

Activity coefficient (γ) for divalent ions	0.36	0.37	0.37	0.37	0.36	0.37	0.37	0.36	0.37	0.36	0.36	0.36	0.36	0.37	0.37	0. 37
(Al^{3+}) [e]$_{gibbsite}$ (mol/L)	$4.37*10^{-13}$	$9.23*10^{-14}$	$1.66*10^{-13}$	$1.95*10^{-14}$	$3.72*10^{-15}$	$1.74*10^{-12}$	$1.78*10^{-13}$	$2.95*10^{-14}$	$3.09*10^{-14}$	$4.47*10^{-15}$	$9.33*10^{-16}$	$4.27*10^{-15}$	$1.26*10^{-16}$	$9.33*10^{-19}$	$2.34*10^{-19}$	$2.24*10^{-20}$
(Al^{3+}) [e]$_{bayerite}$ (mol/L)	$7.25*10^{-12}$	$1.53*10^{-12}$	$2.75*10^{-12}$	$3.24*10^{-13}$	$6.17*10^{-14}$	$2.88*10^{-11}$	$2.95*10^{-12}$	$4.90*10^{-13}$	$5.14*10^{-13}$	$7.41*10^{-14}$	$1.55*10^{-14}$	$7.08*10^{-14}$	$2.09*10^{-15}$	$1.55*10^{-17}$	$3.89*10^{-18}$	$3.72*10^{-19}$
Ksp (gibbsite)	$8.44*10^{-23}$	$8.42*10^{-23}$	$1.91*10^{-22}$	$1.94*10^{-22}$	$1.82*10^{-22}$	$1.95*10^{-22}$	$1.89*10^{-22}$	$1.87*10^{-22}$	$3.76*10^{-22}$	$3.80*10^{-22}$	$3.41*10^{-22}$	$7.71*10^{-22}$	$7.63*10^{-22}$	$1.29*10^{-20}$	$1.30*10^{-20}$	$1.26*10^{-20}$
Average Ksp (gibbsite)	$8.43(\pm0.0097)\times10^{-23}$		$1.89(\pm0.0605)\times10^{-22}$			$1.90(\pm0.0432)\times10^{-22}$			$3.66(\pm0.2137)\times10^{-22}$			$7.67(\pm0.0603)\times10^{-22}$		$1.28(\pm0.0212)\times10^{-20}$		
Ksp (bayerite)	$2.15*10^{-22}$	$2.14*10^{-22}$	$4.88*10^{-22}$	$4.94*10^{-22}$	$4.65*10^{-22}$	$4.98*10^{-22}$	$4.81*10^{-22}$	$4.77*10^{-22}$	$9.59*10^{-22}$	$9.70*10^{-22}$	$8.71*10^{-22}$	$1.97*10^{-21}$	$1.95*10^{-21}$	$3.28*10^{-20}$	$3.30*10^{-20}$	$3.20*10^{-20}$
Average Ksp (bayerite)	$2.15(\pm0.0025)\times10^{-22}$		$4.82(\pm0.1542)\times10^{-22}$			$4.85(\pm0.1103)\times10^{-22}$			$9.33(\pm0.5424)\times10^{-22}$			$1.96(\pm0.0154)\times10^{-21}$		$3.26(\pm0.0451)\times10^{-20}$		

[a] [ ] and ( ) denote concentration and activity, respectively; [ ]*γ=( )

[b] pH measured at equilibrium

[c] [Cl⁻] equals to the NaCl concentration used to control the ionic strength of the system

[d] [Na⁺] comes from the NaCl used as background salt and the NaOH used as titrant for each pH value

[e] (Al^{3+}) in the equilibrium with hydrated γ-Al_2O_3 ; Ksp values are calculated based on different (Al^{3+}) values

Table 3. Comparison of solubility product values (based on the presence of Gibbsite and Bayerite and with and without anion activity) of Me(II)-Al(III)-LDH phases with their corresponding Me(OH)$_2$ phases (Me=Ni, Zn, Co, Fe and Mn)

| Me(II) | Me-Al-LDH | | | | Me(OH)$_2$ |
| | Ksp (with anion activity)[1] | | Ksp (without anion activity)[2] | | |
	Ksp (gibbsite)[1*]	Ksp (bayerite)[1**]	Ksp (gibbsite)[2*]	Ksp (bayerite)[2**]	Ksp
Ni(II)	$8.43(\pm0.0097)\times10^{-23}$	$2.15(\pm0.0025)\times10^{-22}$	$2.00(\pm0.0079)\times10^{-22}$	$5.10(\pm0.0203)\times10^{-22}$	$10^{-17.29}$
	1.58×10^{-24} (Peltier [a]) 8.58×10^{-23} (Regelink [b]) 4.75×10^{-22} (Johnson [c])		1.36×10^{-21} (Regelink [b]) 1.71×10^{-21} (Johnson [c])		
Zn(II)	$1.90(\pm0.0474)\times10^{-22}$	$4.84(\pm0.1209)\times10^{-22}$	$4.48(\pm0.1401)\times10^{-22}$	$1.14(\pm0.0357)\times10^{-21}$	$10^{-16.25}$
	8.58×10^{-22} (Johnson [c])		3.09×10^{-21} (Johnson [c])		
Co(II)	$3.66(\pm0.2137)\times10^{-22}$	$9.33(\pm0.5424)\times10^{-22}$	$8.67(\pm0.4998)\times10^{-22}$	$2.21(\pm0.1272)\times10^{-21}$	$10^{-15.71}$
	4.23×10^{-21} (Johnson [c])		1.52×10^{-20} (Johnson [c])		
Fe(II)	$7.67(\pm0.0603)\times10^{-22}$	$1.96(\pm0.0154)\times10^{-21}$	$1.82(\pm0.0144)\times10^{-21}$	$4.64(\pm0.0368)\times10^{-21}$	$10^{-15.11}$
	$1.21(\pm0.0416)\times10^{-21}$ (Zhu [d])	$2.41(\pm0.0721)\times10^{-21}$	$3.16(\pm0.2930)\times10^{-21}$ (Zhu [d])	$6.27(\pm0.5550)\times10^{-21}$	
Mn(II)	$1.28(\pm0.0212)\times10^{-20}$	$3.26(\pm0.0451)\times10^{-20}$	$3.03(\pm0.0484)\times10^{-20}$	$7.72(\pm0.1233)\times10^{-20}$	$10^{-12.80}$

[1] Ksp values calculated with anion activity ([1*] and [1**] are the values calculated considering the presence of gibbsite and bayerite respectively)

[2] Ksp values calculated without anion activity ([2*] and [2**] are the values calculated considering the presence of gibbsite and bayerite respectively)

[a] converted from Peltier et al., 2006, *Clays and Clay Minerals*

[b] converted from Johnson and Glasser, 2003, *Clays and Clay Minerals*

[c] converted from Regelink and Temminghoff, 2011, *Environmental Pollution*

[d] taken from Zhu and Elzinga, 2014, *Environmental Science & Technology*

Table 4. Composition of model groundwater (from Tang and Johannesson, 2003).

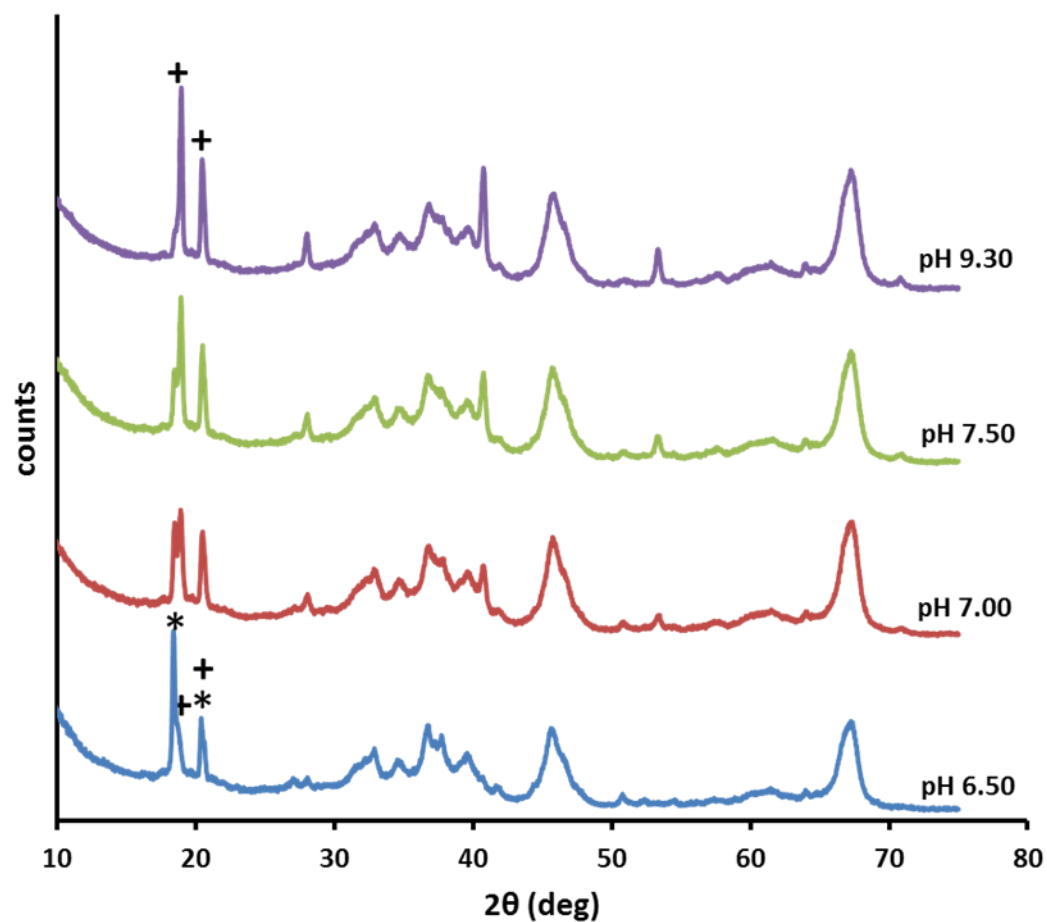| Solute	Concentration (mM)
HCO_3	0.957
SO_4	0.117
NO_3	0.100
Cl	0.22
Na	0.74
K	0.059
Ca	0.375
Mg	0.171
Fe	0.012

Appendix B: Figures

Figure 1. XRD patterns of the equilibrium hydrated products of adsorbent γ-Al$_2$O$_3$ used in this experiment. Hydration carried over the entire range of pH values used for this study from pH 6.50-9.30, γ-Al$_2$O$_3$ suspension density is 5.0 g L^{-1}.(*) gibbsite; (+) bayerite
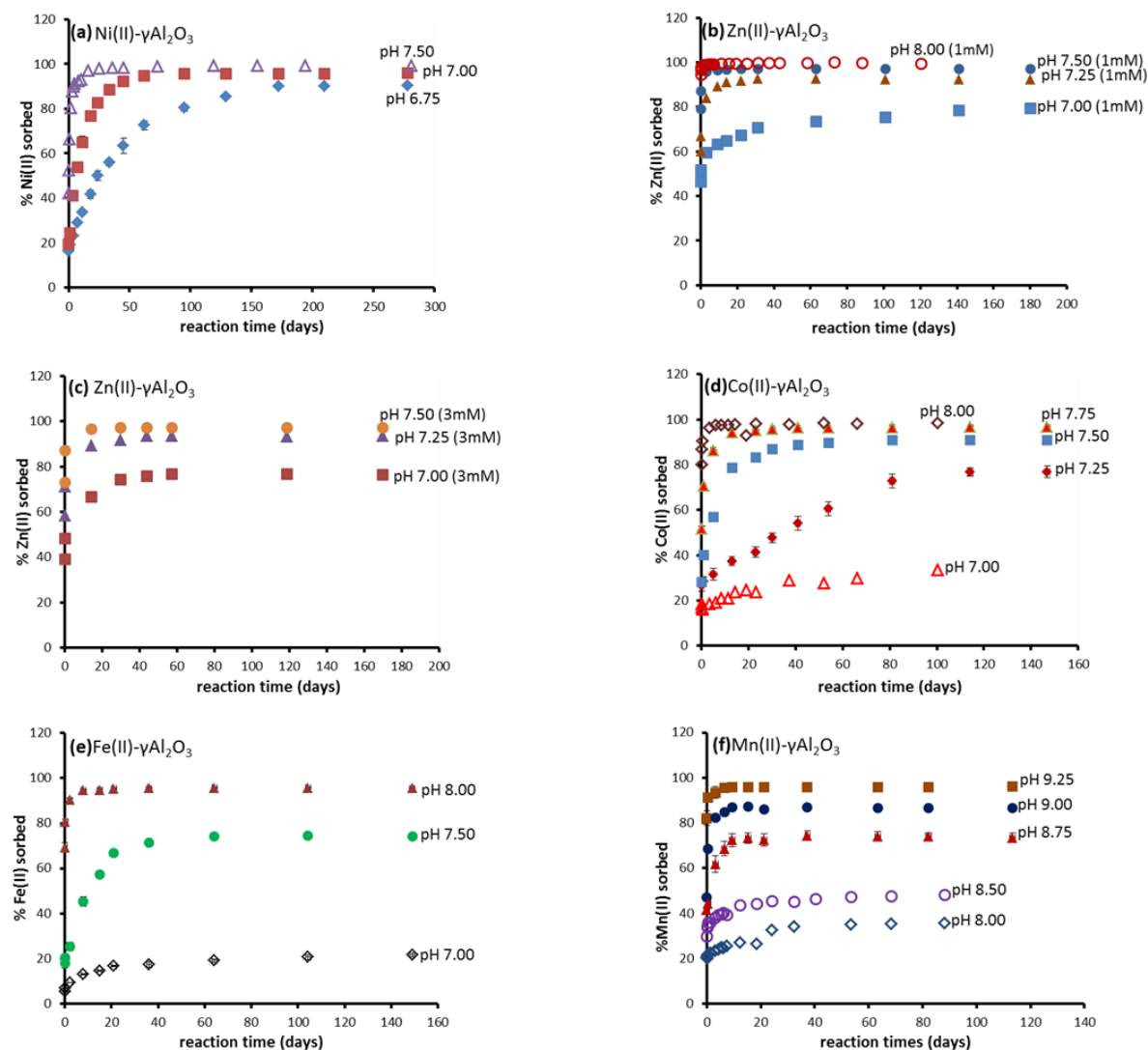
Figure 2. Kinetics of (a) Ni(II) , (b) and (c) Zn(II), (d) Co(II), (e) Fe(II) and (f) Mn(II) sorption in anoxic suspension of γ-Al$_2$O$_3$. The aqueous Me(II) concentration was 1.0 mM (1.0 mM and 3.0 mM for Zn(II)-γAl$_2$O$_3$ system) and the aluminum oxide suspension density was 5.0 g L^{-1}. The closed and open symbols respectively denote the pH values used and discarded for the calculation of Ksp for each metal.
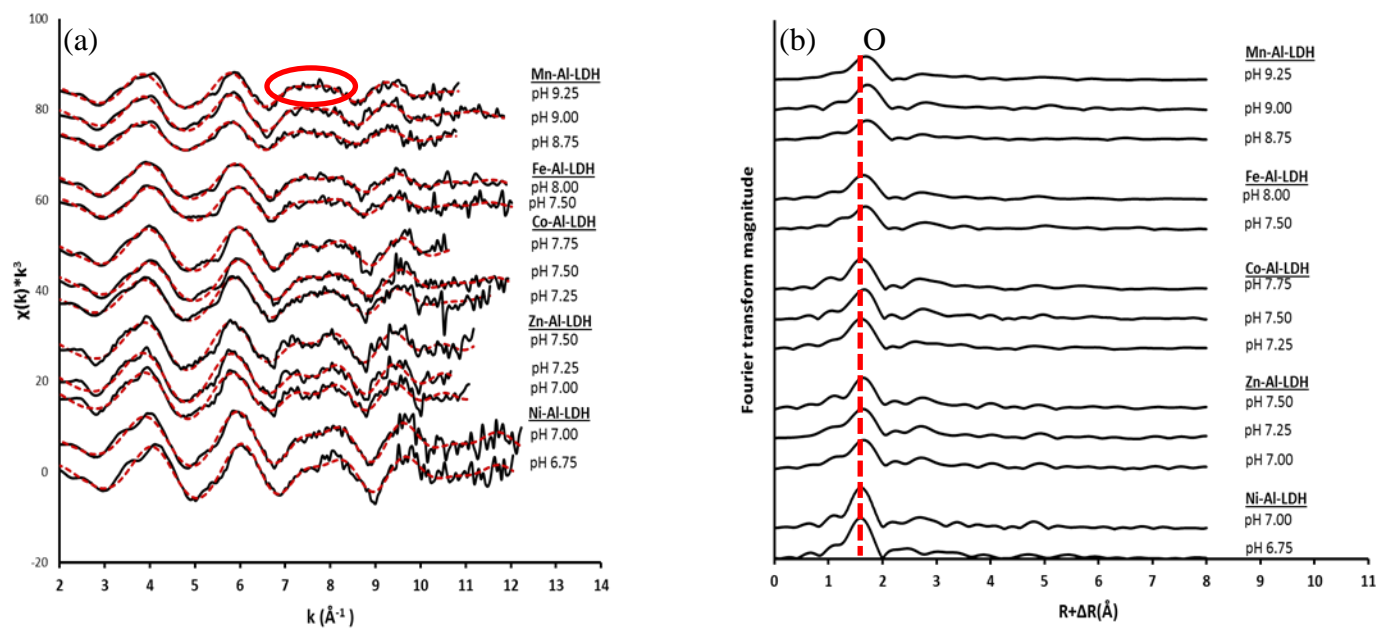
Figure 3. EXAFS data of the Me(II)-Al(III)-LDH (Me= Ni, Zn, Co, Fe, Mn) phases:(a) raw (solid lines) and fitted (dotted lines) k^3-weighted χ functions; (b) corresponding radial structure functions of the raw spectra (RSFs). The red circle in the top χ spectrum in panel a identifies the fingerprint oscillation of Me(II)-Al(III)-LDH phases and the red dotted line in panel b indicates the atomic neighbors.
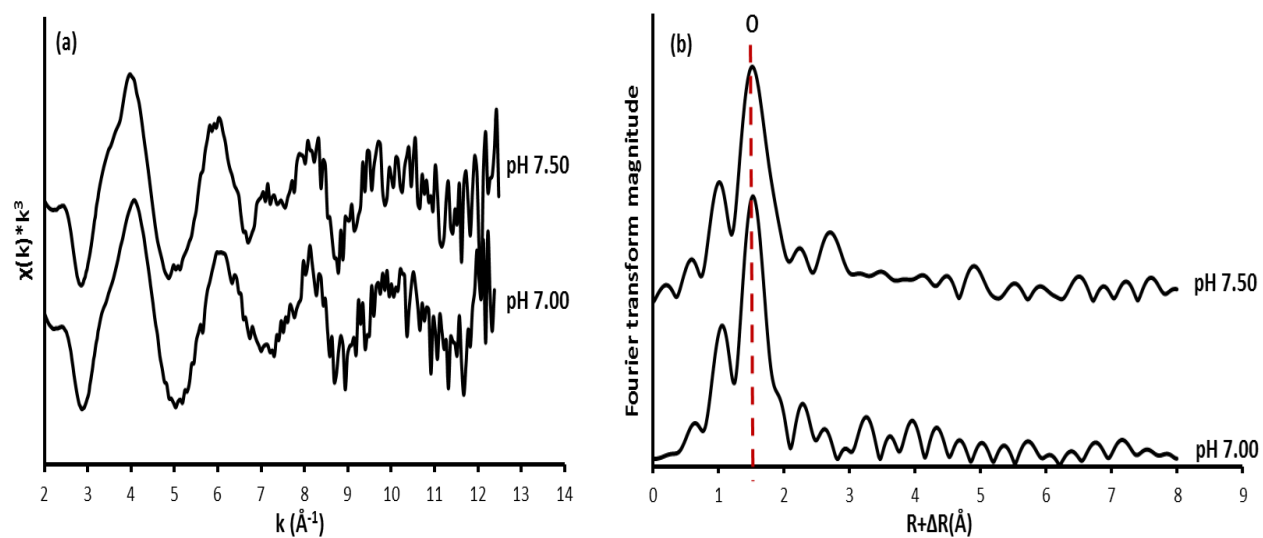
Figure 4. EXAFS data of the Zn(II)- γAl$_2$O$_3$ system at aqueous [Zn(II)] =1mM and pH =7.00, 7.50 : (a) raw k^3-weighted χ functions; (b) corresponding radial structure functions of the raw spectra (RSFs). The red dotted line in panel b indicates the atomic neighbors.
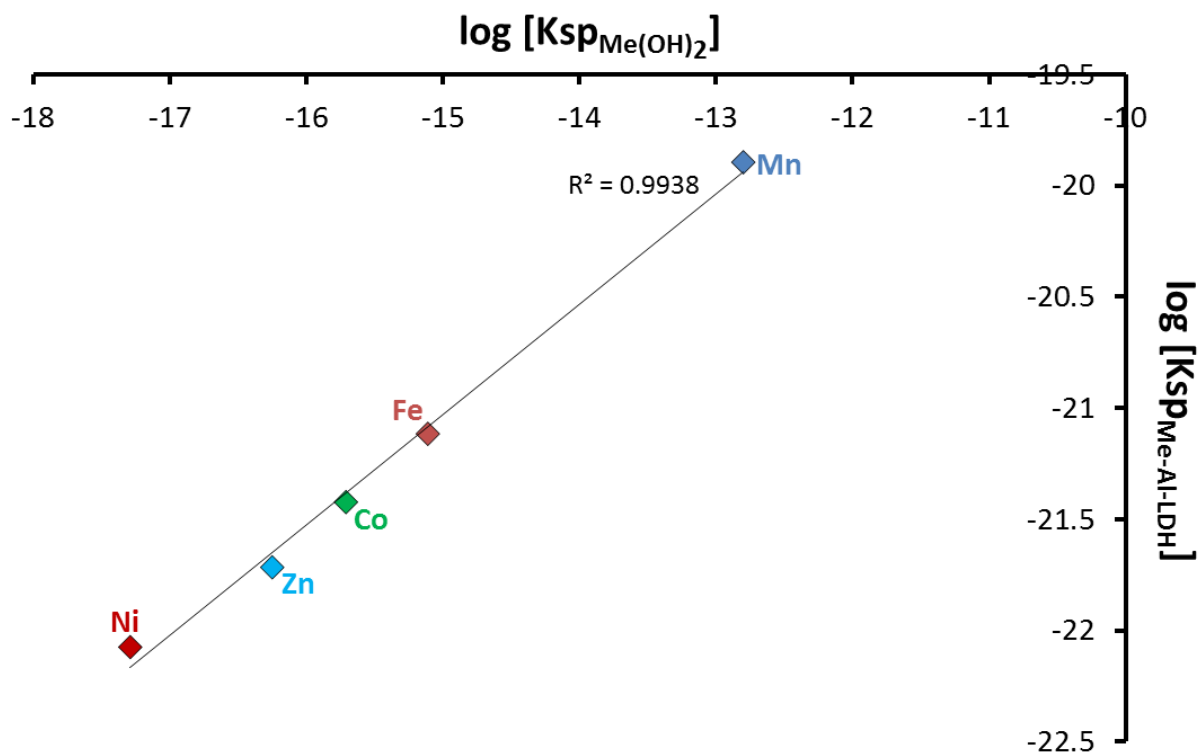
Figure 5. Comparison of solubility product values of Me(II)-Al(III)-LDH phases with their corresponding Me(OH)$_2$s (Me= Ni, Zn, Co, Fe, Mn).
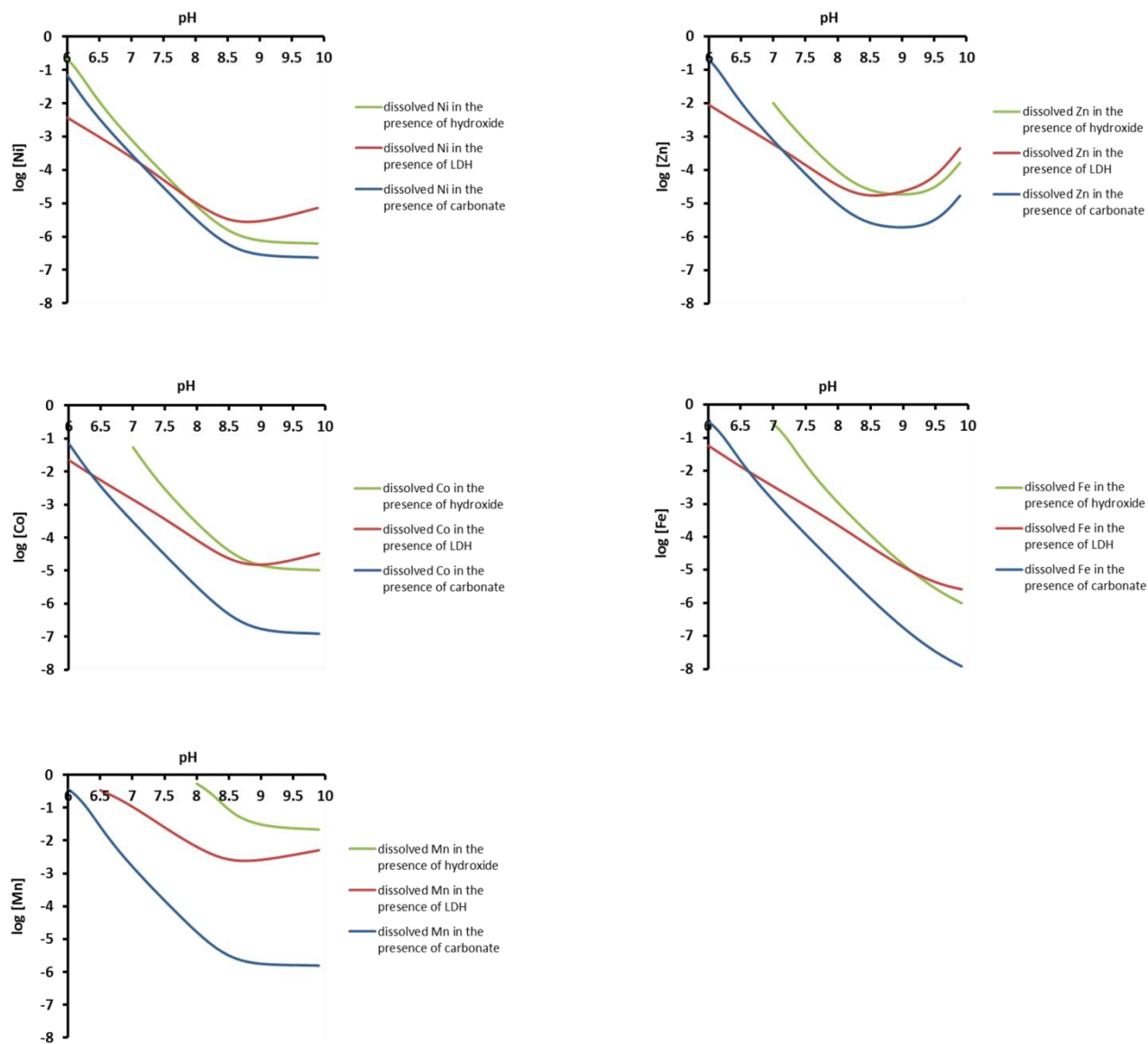
Figure 6. Dissolved Me(II) (Me= Ni, Zn, Co, Fe, Mn) concentration values in a model groundwater system in the presence of corresponding Me(OH)$_2$, Me-Al-LDH and MeCO$_3$ phases over a pH range of 6.0-10.0.
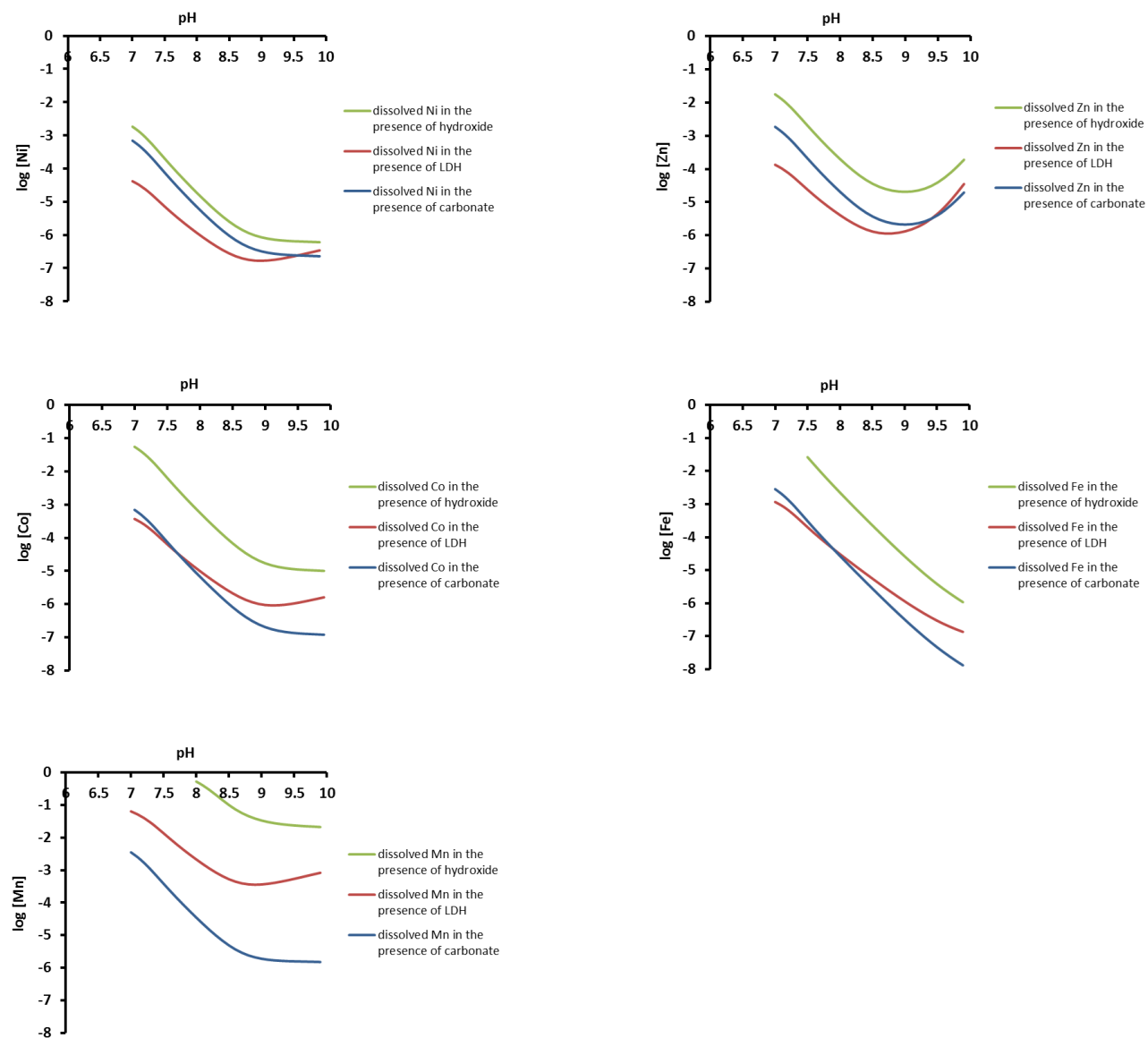
Figure 7. Dissolved Me(II) (Me= Ni, Zn, Co, Fe, Mn) concentration values in calcitic system in the presence of corresponding Me(OH)$_2$, Me-Al-LDH and MeCO$_3$ phases over a pH range of 6.0-10.0.